Observation of a near-threshold enhancement in the $\Lambda\bar{\Lambda}$ mass spectrum from $e^+e^- \to \phi\Lambda\bar{\Lambda}$ at $\sqrt{s}$ from 3.51 to 4.60 GeV

M. Ablikim,[1] M. N. Achasov,[10,c] P. Adlarson,[67] S. Ahmed,[15] M. Albrecht,[4] R. Aliberti,[28] A. Amoroso,[66a,66c] M. R. An,[32] Q. An,[63,49] X. H. Bai,[57] Y. Bai,[48] O. Bakina,[29] R. Baldini Ferroli,[23a] I. Balossino,[24a] Y. Ban,[38,k] K. Begzsuren,[26] N. Berger,[28] M. Bertani,[23a] D. Bettoni,[24a] F. Bianchi,[66a,66c] J. Bloms,[60] A. Bortone,[66a,66c] I. Boyko,[29] R. A. Briere,[5] H. Cai,[68] X. Cai,[1,49] A. Calcaterra,[23a] G. F. Cao,[1,54] N. Cao,[1,54] S. A. Cetin,[53a] J. F. Chang,[1,49] W. L. Chang,[1,54] G. Chelkov,[29,b] D. Y. Chen,[6] G. Chen,[1] H. S. Chen,[1,54] M. L. Chen,[1,49] S. J. Chen,[35] X. R. Chen,[25] Y. B. Chen,[1,49] Z. J. Chen,[20,l] W. S. Cheng,[66c] G. Cibinetto,[24a] F. Cossio,[66c] X. F. Cui,[36] H. L. Dai,[1,49] X. C. Dai,[1,54] A. Dbeyssi,[15] R. E. de Boer,[4] D. Dedovich,[29] Z. Y. Deng,[1] A. Denig,[28] I. Denysenko,[29] M. Destefanis,[66a,66c] F. De Mori,[66a,66c] Y. Ding,[33] C. Dong,[36] J. Dong,[1,49] L. Y. Dong,[1,54] M. Y. Dong,[1,49,54] X. Dong,[68] S. X. Du,[71] Y. L. Fan,[68] J. Fang,[1,49] S. S. Fang,[1,54] Y. Fang,[1] R. Farinelli,[24a] L. Fava,[66b,66c] F. Feldbauer,[4] G. Felici,[23a] C. Q. Feng,[63,49] J. H. Feng,[50] M. Fritsch,[4] C. D. Fu,[1] Y. Gao,[63,49] Y. Gao,[38,k] Y. Gao,[64] Y. G. Gao,[6] I. Garzia,[24a,24b] P. T. Ge,[68] C. Geng,[50] E. M. Gersabeck,[58] A. Gilman,[61] K. Goetzen,[11] L. Gong,[33] W. X. Gong,[1,49] W. Gradl,[28] M. Greco,[66a,66c] L. M. Gu,[35] M. H. Gu,[1,49] S. Gu,[2] Y. T. Gu,[13] C. Y. Guan,[1,54] A. Q. Guo,[22] L. B. Guo,[34] R. P. Guo,[40] Y. P. Guo,[9,h] A. Guskov,[29] T. T. Han,[41] W. Y. Han,[32] X. Q. Hao,[16] F. A. Harris,[56] N. Hüsken,[22,28] K. L. He,[1,54] F. H. Heinsius,[4] C. H. Heinz,[28] T. Held,[4] Y. K. Heng,[1,49,54] C. Herold,[51] M. Himmelreich,[11,f] T. Holtmann,[4] Y. R. Hou,[54] Z. L. Hou,[1] H. M. Hu,[1,54] J. F. Hu,[47,m] T. Hu,[1,49,54] Y. Hu,[1] G. S. Huang,[63,49] L. Q. Huang,[64] X. T. Huang,[41] Y. P. Huang,[1] Z. Huang,[38,k] T. Hussain,[65] W. Ikegami Andersson,[67] W. Imoehl,[22] M. Irshad,[63,49] S. Jaeger,[4] S. Janchiv,[26,j] Q. Ji,[1] Q. P. Ji,[16] X. B. Ji,[1,54] X. L. Ji,[1,49] Y. Y. Ji,[41] H. B. Jiang,[41] X. S. Jiang,[1,49,54] J. B. Jiao,[41] Z. Jiao,[18] S. Jin,[35] Y. Jin,[57] T. Johansson,[67] N. Kalantar-Nayestanaki,[55] X. S. Kang,[33] R. Kappert,[55] M. Kavatsyuk,[55] B. C. Ke,[43,1] I. K. Keshk,[4] A. Khoukaz,[60] P. Kiese,[28] R. Kiuchi,[1] R. Kliemt,[11] L. Koch,[30] O. B. Kolcu,[53a,e] B. Kopf,[4] M. Kuemmel,[4] M. Kuessner,[4] A. Kupsc,[67] M. G. Kurth,[1,54] W. Kühn,[30] J. J. Lane,[58] J. S. Lange,[30] P. Larin,[15] A. Lavania,[21] L. Lavezzi,[66a,66c] Z. H. Lei,[63,49] H. Leithoff,[28] M. Lellmann,[28] T. Lenz,[28] C. Li,[39] C. H. Li,[32] Cheng Li,[63,49] D. M. Li,[71] F. Li,[1,49] G. Li,[1] H. Li,[63,49] H. Li,[43] H. B. Li,[1,54] H. J. Li,[16] J. L. Li,[41] J. Q. Li,[4] J. S. Li,[50] Ke Li,[1] L. K. Li,[1] Lei Li,[3] P. R. Li,[31] S. Y. Li,[52] W. D. Li,[1,54] W. G. Li,[1] X. H. Li,[63,49] X. L. Li,[41] Xiaoyu Li,[1,54] Z. Y. Li,[50] H. Liang,[1,54] H. Liang,[63,49] H. Liang,[27] Y. F. Liang,[45] Y. T. Liang,[25] G. R. Liao,[12] L. Z. Liao,[1,54] J. Libby,[21] C. X. Lin,[50] B. J. Liu,[1] C. X. Liu,[1] D. Liu,[63,49] F. H. Liu,[44] Fang Liu,[1] Feng Liu,[6] H. B. Liu,[13] H. M. Liu,[1,54] Huanhuan Liu,[1] Huihui Liu,[17] J. B. Liu,[63,49] J. L. Liu,[64] J. Y. Liu,[1,54] K. Liu,[1] K. Y. Liu,[33] Ke Liu,[6] L. Liu,[63,49] M. H. Liu,[9,h] P. L. Liu,[1] Q. Liu,[54] Q. Liu,[68] S. B. Liu,[63,49] Shuai Liu,[46] T. Liu,[1,54] W. M. Liu,[63,49] X. Liu,[31] Y. Liu,[31] Y. B. Liu,[36] Z. A. Liu,[1,49,54] Z. Q. Liu,[41] X. C. Lou,[1,49,54] F. X. Lu,[50] H. J. Lu,[18] J. D. Lu,[1,54] J. G. Lu,[1,49] X. L. Lu,[1] Y. Lu,[1] Y. P. Lu,[1,49] C. L. Luo,[34] M. X. Luo,[70] P. W. Luo,[50] T. Luo,[9,h] X. L. Luo,[1,49] X. R. Lyu,[54] F. C. Ma,[33] H. L. Ma,[1] L. L. Ma,[41] M. M. Ma,[1,54] Q. M. Ma,[1] R. Q. Ma,[1,54] R. T. Ma,[54] X. X. Ma,[1,54] X. Y. Ma,[1,49] F. E. Maas,[15] M. Maggiora,[66a,66c] S. Maldaner,[4] S. Malde,[61] Q. A. Malik,[65] A. Mangoni,[23b] Y. J. Mao,[38,k] Z. P. Mao,[1] S. Marcello,[66a,66c] Z. X. Meng,[57] J. G. Messchendorp,[55] G. Mezzadri,[24a] T. J. Min,[35] R. E. Mitchell,[22] X. H. Mo,[1,49,54] Y. J. Mo,[6] N. Yu. Muchnoi,[10,c] H. Muramatsu,[59] S. Nakhoul,[11,f] Y. Nefedov,[29] F. Nerling,[11,f] I. B. Nikolaev,[10,c] Z. Ning,[1,49] S. Nisar,[8,i] S. L. Olsen,[54] Q. Ouyang,[1,49,54] S. Pacetti,[23b,23c] X. Pan,[9,h] Y. Pan,[58] A. Pathak,[1] P. Patteri,[23a] M. Pelizaeus,[4] H. P. Peng,[63,49] K. Peters,[11,f] J. Pettersson,[67] J. L. Ping,[34] R. G. Ping,[1,54] R. Poling,[59] V. Prasad,[63,49] H. Qi,[63,49] H. R. Qi,[52] K. H. Qi,[25] M. Qi,[35] T. Y. Qi,[9] T. Y. Qi,[2] S. Qian,[1,49] W. B. Qian,[54] Z. Qian,[50] C. F. Qiao,[54] L. Q. Qin,[12] X. P. Qin,[9] X. S. Qin,[41] Z. H. Qin,[1,49] J. F. Qiu,[1] S. Q. Qu,[36] K. H. Rashid,[65] K. Ravindran,[21] C. F. Redmer,[28] A. Rivetti,[66c] V. Rodin,[55] M. Rolo,[66c] G. Rong,[1,54] Ch. Rosner,[15] M. Rump,[60] H. S. Sang,[63] A. Sarantsev,[29,d] Y. Schelhaas,[28] C. Schnier,[4] K. Schoenning,[67] M. Scodeggio,[24a,24b] D. C. Shan,[46] W. Shan,[19] X. Y. Shan,[63,49] J. F. Shangguan,[46] M. Shao,[63,49] C. P. Shen,[9] P. X. Shen,[36] X. Y. Shen,[1,54] H. C. Shi,[63,49] R. S. Shi,[1,54] X. Shi,[1,49] X. D. Shi,[63,49] J. J. Song,[41] W. M. Song,[27,1] Y. X. Song,[38,k] S. Sosio,[66a,66c] S. Spataro,[66a,66c] K. X. Su,[68] P. P. Su,[46] F. F. Sui,[41] G. X. Sun,[1] H. K. Sun,[1] J. F. Sun,[16] L. Sun,[68] S. S. Sun,[1,54] T. Sun,[1,54] W. Y. Sun,[34] W. Y. Sun,[27] X. Sun,[20,l] Y. J. Sun,[63,49] Y. K. Sun,[63,49] Y. Z. Sun,[1] Z. T. Sun,[1] Y. H. Tan,[68] Y. X. Tan,[63,49] C. J. Tang,[45] G. Y. Tang,[1] J. Tang,[50] J. X. Teng,[63,49] V. Thoren,[67] W. H. Tian,[43] Y. T. Tian,[25] I. Uman,[53b] B. Wang,[1] C. W. Wang,[35] D. Y. Wang,[38,k] H. J. Wang,[31] H. P. Wang,[1,54] K. Wang,[1,49] L. L. Wang,[1] M. Wang,[41] M. Z. Wang,[38,k] Meng Wang,[1,54] W. Wang,[50] W. H. Wang,[68] W. P. Wang,[63,49] X. Wang,[38,k] X. F. Wang,[31] X. L. Wang,[9,h] Y. Wang,[50] Y. Wang,[63,49] Y. D. Wang,[37] Y. F. Wang,[1,49,54] Y. Q. Wang,[1] Y. Y. Wang,[31] Z. Wang,[1,49] Z. Y. Wang,[1] Ziyi Wang,[54] Zongyuan Wang,[1,54] D. H. Wei,[12] F. Weidner,[60] S. P. Wen,[1] D. J. White,[58] U. Wiedner,[4] G. Wilkinson,[61] M. Wolke,[67] L. Wollenberg,[4] J. F. Wu,[1,54] L. H. Wu,[1] L. J. Wu,[1,54] X. Wu,[9,h] Z. Wu,[1,49] L. Xia,[63,49] H. Xiao,[9,h] S. Y. Xiao,[1] Z. J. Xiao,[34] X. H. Xie,[38,k] Y. G. Xie,[1,49] Y. H. Xie,[6] T. Y. Xing,[1,54] G. F. Xu,[1] Q. J. Xu,[14] W. Xu,[1,54] X. P. Xu,[46] Y. C. Xu,[54] F. Yan,[9,h] L. Yan,[9,h] W. B. Yan,[63,49] W. C. Yan,[71] Xu Yan,[46] H. J. Yang,[42,g] H. X. Yang,[1] L. Yang,[43] S. L. Yang,[54] Y. X. Yang,[12] Yifan Yang,[1,54] Zhi Yang,[25] M. Ye,[1,49] M. H. Ye,[7] J. H. Yin,[1] Z. Y. You,[50] B. X. Yu,[1,49,54] C. X. Yu,[36] G. Yu,[1,54] J. S. Yu,[20,l] T. Yu,[64] C. Z. Yuan,[1,54] L. Yuan,[2] X. Q. Yuan,[38,k] Y. Yuan,[1] Z. Y. Yuan,[50] C. X. Yue,[32] A. Yuncu,[53a,a] A. A. Zafar,[65]

Y. Zeng,[20,l] B. X. Zhang,[1] Guangyi Zhang,[16] H. Zhang,[63] H. H. Zhang,[50] H. H. Zhang,[27] H. Y. Zhang,[1,49] J. J. Zhang,[43] J. L. Zhang,[69] J. Q. Zhang,[34] J. W. Zhang,[1,49,54] J. Y. Zhang,[1] J. Z. Zhang,[1,54] Jianyu Zhang,[1,54] Jiawei Zhang,[1,54] L. M. Zhang,[52] L. Q. Zhang,[50] Lei Zhang,[35] S. Zhang,[50] S. F. Zhang,[35] Shulei Zhang,[20,l] X. Zhang,[36] X. D. Zhang,[37] X. Y. Zhang,[41] Y. Zhang,[61] Y. H. Zhang,[1,49] Y. T. Zhang,[63,49] Yan Zhang,[63,49] Yao Zhang,[1] Yi Zhang,[9,h] Z. H. Zhang,[6] Z. Y. Zhang,[68] G. Zhao,[1] J. Zhao,[32] J. Y. Zhao,[1,54] J. Z. Zhao,[1,49] Lei Zhao,[63,49] Ling Zhao,[1] M. G. Zhao,[36] Q. Zhao,[1] S. J. Zhao,[71] Y. B. Zhao,[1,49] Y. X. Zhao,[25] Z. G. Zhao,[63,49] A. Zhemchugov,[29,b] B. Zheng,[64] J. P. Zheng,[1,49] Y. Zheng,[38,k] Y. H. Zheng,[54] B. Zhong,[34] C. Zhong,[64] L. P. Zhou,[1,54] Q. Zhou,[1,54] X. Zhou,[68] X. K. Zhou,[54] X. R. Zhou,[63,49] X. Y. Zhou,[32] A. N. Zhu,[1,54] J. Zhu,[36] K. Zhu,[1] K. J. Zhu,[1,49,54] S. H. Zhu,[62] T. J. Zhu,[69] W. J. Zhu,[9,h] W. J. Zhu,[36] Y. C. Zhu,[63,49] Z. A. Zhu,[1,54] B. S. Zou,[1] and J. H. Zou[1]

(BESIII Collaboration)

[1]*Institute of High Energy Physics, Beijing 100049, People's Republic of China*
[2]*Beihang University, Beijing 100191, People's Republic of China*
[3]*Beijing Institute of Petrochemical Technology, Beijing 102617, People's Republic of China*
[4]*Bochum Ruhr-University, D-44780 Bochum, Germany*
[5]*Carnegie Mellon University, Pittsburgh, Pennsylvania 15213, USA*
[6]*Central China Normal University, Wuhan 430079, People's Republic of China*
[7]*China Center of Advanced Science and Technology, Beijing 100190, People's Republic of China*
[8]*COMSATS University Islamabad, Lahore Campus, Defence Road, Off Raiwind Road,*
54000 Lahore, Pakistan
[9]*Fudan University, Shanghai 200443, People's Republic of China*
[10]*G.I. Budker Institute of Nuclear Physics SB RAS (BINP), Novosibirsk 630090, Russia*
[11]*GSI Helmholtzcentre for Heavy Ion Research GmbH, D-64291 Darmstadt, Germany*
[12]*Guangxi Normal University, Guilin 541004, People's Republic of China*
[13]*Guangxi University, Nanning 530004, People's Republic of China*
[14]*Hangzhou Normal University, Hangzhou 310036, People's Republic of China*
[15]*Helmholtz Institute Mainz, Staudinger Weg 18, D-55099 Mainz, Germany*
[16]*Henan Normal University, Xinxiang 453007, People's Republic of China*
[17]*Henan University of Science and Technology, Luoyang 471003, People's Republic of China*
[18]*Huangshan College, Huangshan 245000, People's Republic of China*
[19]*Hunan Normal University, Changsha 410081, People's Republic of China*
[20]*Hunan University, Changsha 410082, People's Republic of China*
[21]*Indian Institute of Technology Madras, Chennai 600036, India*
[22]*Indiana University, Bloomington, Indiana 47405, USA*
[23a]*INFN Laboratori Nazionali di Frascati, I-00044 Frascati, Italy*
[23b]*INFN Laboratori Nazionali di Frascati, INFN Sezione di Perugia, I-06100 Perugia, Italy*
[23c]*INFN Laboratori Nazionali di Frascati, University of Perugia, I-06100 Perugia, Italy*
[24a]*INFN Sezione di Ferrara, I-44122 Ferrara, Italy*
[24b]*INFN Sezione di Ferrara, University of Ferrara, I-44122 Ferrara, Italy*
[25]*Institute of Modern Physics, Lanzhou 730000, People's Republic of China*
[26]*Institute of Physics and Technology, Peace Avenue 54B, Ulaanbaatar 13330, Mongolia*
[27]*Jilin University, Changchun 130012, People's Republic of China*
[28]*Johannes Gutenberg University of Mainz, Johann-Joachim-Becher-Weg 45, D-55099 Mainz, Germany*
[29]*Joint Institute for Nuclear Research, 141980 Dubna, Moscow region, Russia*
[30]*Justus-Liebig-Universitaet Giessen, II. Physikalisches Institut, Heinrich-Buff-Ring 16,*
D-35392 Giessen, Germany
[31]*Lanzhou University, Lanzhou 730000, People's Republic of China*
[32]*Liaoning Normal University, Dalian 116029, People's Republic of China*
[33]*Liaoning University, Shenyang 110036, People's Republic of China*
[34]*Nanjing Normal University, Nanjing 210023, People's Republic of China*
[35]*Nanjing University, Nanjing 210093, People's Republic of China*
[36]*Nankai University, Tianjin 300071, People's Republic of China*
[37]*North China Electric Power University, Beijing 102206, People's Republic of China*
[38]*Peking University, Beijing 100871, People's Republic of China*
[39]*Qufu Normal University, Qufu 273165, People's Republic of China*
[40]*Shandong Normal University, Jinan 250014, People's Republic of China*
[41]*Shandong University, Jinan 250100, People's Republic of China*
[42]*Shanghai Jiao Tong University, Shanghai 200240, People's Republic of China*

[43]*Shanxi Normal University, Linfen 041004, People's Republic of China*
[44]*Shanxi University, Taiyuan 030006, People's Republic of China*
[45]*Sichuan University, Chengdu 610064, People's Republic of China*
[46]*Soochow University, Suzhou 215006, People's Republic of China*
[47]*South China Normal University, Guangzhou 510006, People's Republic of China*
[48]*Southeast University, Nanjing 211100, People's Republic of China*
[49]*State Key Laboratory of Particle Detection and Electronics, Beijing 100049,*
Hefei 230026, People's Republic of China
[50]*Sun Yat-Sen University, Guangzhou 510275, People's Republic of China*
[51]*Suranaree University of Technology, University Avenue 111, Nakhon Ratchasima 30000, Thailand*
[52]*Tsinghua University, Beijing 100084, People's Republic of China*
[53a]*Turkish Accelerator Center Particle Factory Group, Istanbul Bilgi University,*
34060 Eyup, Istanbul, Turkey;
[53b]*Near East University, Nicosia, North Cyprus, Mersin 10, Turkey*
[54]*University of Chinese Academy of Sciences, Beijing 100049, People's Republic of China*
[55]*University of Groningen, NL-9747 AA Groningen, The Netherlands*
[56]*University of Hawaii, Honolulu, Hawaii 96822, USA*
[57]*University of Jinan, Jinan 250022, People's Republic of China*
[58]*University of Manchester, Oxford Road, Manchester M13 9PL, United Kingdom*
[59]*University of Minnesota, Minneapolis, Minnesota 55455, USA*
[60]*University of Muenster, Wilhelm-Klemm-Straße 9, 48149 Muenster, Germany*
[61]*University of Oxford, Keble Rd, Oxford OX13RH, United Kingdom*
[62]*University of Science and Technology Liaoning, Anshan 114051, People's Republic of China*
[63]*University of Science and Technology of China, Hefei 230026, People's Republic of China*
[64]*University of South China, Hengyang 421001, People's Republic of China*
[65]*University of the Punjab, Lahore-54590, Pakistan*
[66a]*University of Turin, I-10125 Turin, Italy*
[66b]*University of Turin and INFN, University of Eastern Piedmont, I-15121 Alessandria, Italy*
[66c]*University of Turin and INFN, INFN, I-10125 Turin, Italy*
[67]*Uppsala University, Box 516, SE-75120 Uppsala, Sweden*
[68]*Wuhan University, Wuhan 430072, People's Republic of China*
[69]*Xinyang Normal University, Xinyang 464000, People's Republic of China*
[70]*Zhejiang University, Hangzhou 310027, People's Republic of China*
[71]*Zhengzhou University, Zhengzhou 450001, People's Republic of China*

The process $e^+e^- \to \phi\Lambda\bar{\Lambda}$ is studied using data samples collected with the BESIII detector at the BEPCII Collider at center of mass energies $\sqrt{s}$ ranging from 3.51 GeV to 4.60 GeV. An enhancement is observed near the threshold of $\Lambda\bar{\Lambda}$. The lineshape of this enhancement is studied in different approaches,

[a]Also at Bogazici University, 34342 Istanbul, Turkey.
[b]Also at the Moscow Institute of Physics and Technology, Moscow 141700, Russia.
[c]Also at the Novosibirsk State University, Novosibirsk 630090, Russia.
[d]Also at the NRC "Kurchatov Institute", PNPI, 188300 Gatchina, Russia.
[e]Also at Istanbul Arel University, 34295 Istanbul, Turkey.
[f]Also at Goethe University Frankfurt, 60323 Frankfurt am Main, Germany.
[g]Also at Key Laboratory for Particle Physics, Astrophysics and Cosmology, Ministry of Education; Shanghai Key Laboratory for Particle Physics and Cosmology; Institute of Nuclear and Particle Physics, Shanghai 200240, People's Republic of China.
[h]Also at Key Laboratory of Nuclear Physics and Ion-beam Application (MOE) and Institute of Modern Physics, Fudan University, Shanghai 200443, People's Republic of China.
[i]Also at Harvard University, Department of Physics, Cambridge, Massachusetts 02138, USA.
[j]Present address: Institute of Physics and Technology, Peace Avenue 54B, Ulaanbaatar 13330, Mongolia.
[k]Also at State Key Laboratory of Nuclear Physics and Technology, Peking University, Beijing 100871, People's Republic of China.
[l]School of Physics and Electronics, Hunan University, Changsha 410082, People's Republic of China.
[m]Also at Guangdong Provincial Key Laboratory of Nuclear Science, Institute of Quantum Matter, South China Normal University, Guangzhou 510006, People's Republic of China.

including fit with a Breit-Wigner function or a reversed exponential function. The Breit-Wigner function has a mass of $(2262 \pm 4 \pm 28)$ MeV/c^2 and a width of $(72 \pm 5 \pm 43)$ MeV, where the quoted uncertainties are statistical and systematic, respectively. The rising rate of the reversed exponential function is measured as $33 \pm 11 \pm 6$ MeV/c^2. For the $\Lambda\bar{\Lambda}$ system, the J^{PC} quantum numbers of 0^{-+} and 0^{++} are rejected, while other J^{PC} hypotheses are possible, according to the helicity-angle study. The energy-dependent cross section of the $e^+e^- \to \phi\Lambda\bar{\Lambda}$ process is measured for the first time in this energy region, and contributions from excited ψ states and vector charmoniumlike Y-states are investigated.

I. INTRODUCTION

Early in this 21st century, a number of exotic states were discovered [1] in final states with a quarkonium and one or two light hadrons, or with heavy-flavor mesons. Among these states, there are vector states with $J^{PC} = 1^{--}$ which are usually called Y states, such as the $Y(4260)$ [2], $Y(4360)$ [3,4], and $Y(4660)$ [3]. The $Y(4260)$ state is observed for the first time by the *BABAR* experiment with a mass of $(4259 \pm 8^{+2}_{-6})$ MeV/c^2 using the initial state radiation (ISR) events $e^+e^- \to \gamma_{\text{ISR}}\pi^+\pi^- J/\psi$ [2]. The observation was latter confirmed by the CLEO [5] and Belle experiments [6]. In 2017, a dedicated analysis performed by the BESIII experiment revealed that the so-called $Y(4260)$ state is not simply one Breit-Wigner (BW) resonance and can be a combination of two states [7]. The first one has a lower mass and a much narrower width than the $Y(4260)$, but is consistent with the $Y(4220)$ state observed in $e^+e^- \to \pi^+\pi^- h_c$ events [8,9], and the second one at around 4.32 GeV/c^2 was observed for the first time with a significance greater than 7.6σ. The lower-mass resonance was also observed in $e^+e^- \to \omega\chi_{c0}$ [10] and $\pi\bar{D}D^*$ + c.c. events [11].

Until now, the $Y(4260)$ and other vector charmoniumlike states were only reported in final states containing a $c\bar{c}$ pair: either charmonium states or charmed mesons. Several analyses have been performed by the BESIII Collaboration to search for light hadron decays of these states, for example, $Y(4260) \to \pi^0(\eta)p\bar{p}$ [12], $K^+K^-\pi^0$ [13], $\Xi\bar{\Xi}$ [14], etc. Although there is no significant contribution from the vector charmonium or charmonium-like states identified, the cross section line shapes of these processes do suggest contributions from amplitudes beyond simple continuum production. In Ref. [15], the $Y(4260)$ state is interpreted as a diquark-antidiquark state ($[cs][\bar{c}\,\bar{s}]$). This interpretation implies that the $Y(4260)$ state decays easily into final states containing a pair of $s\bar{s}$. One of the dominant contributions to $e^+e^- \to \pi^+\pi^- J/\psi$ comes from $Y(4260) \to f_0(980)J/\psi$ decays [16], and the $f_0(980)$ meson is known to have a large $s\bar{s}$ component. If the $c\bar{c}$ quarks in $Y(4260)$ annihilate while the $s\bar{s}$ pair survives in the final state, we expect $Y(4260)$ decays into strange mesons or baryons, such as $\phi\Lambda\bar{\Lambda}$. Such a signal will manifest itself as a line shape distortion due to the interference between the amplitudes of the $Y(4260)$ decay and the $e^+e^- \to \phi\Lambda\bar{\Lambda}$ continuum production.

The $\eta(2225)$ and $\phi(2170)$ states [17] are interpreted as loosely bound states of $\Lambda\bar{\Lambda}$ in Ref. [18]. This suggests that the $\eta(2225)$ couples to $\Lambda\bar{\Lambda}$ strongly above the threshold and it can be produced in $e^+e^- \to \phi\Lambda\bar{\Lambda}$ processes. Together with the strong enhancement of the $e^+e^- \to \Lambda\bar{\Lambda}$ production cross section close to threshold [19], this can help establish if there is any connection between these two hadron molecule candidates. On the other hand, near-threshold enhancements are observed in several processes involving baryon/antibaryon pairs such as $J/\psi \to \gamma p\bar{p}$ [20], $B \to Kp\bar{p}$ [21], and $B^0 \to K\Lambda\bar{\Lambda}$ [22]. There are a few interpretations for these phenomena, including states near the threshold as found in a model by Nambu and Jona-Lasinio [23], $J^{PC} = 0^{\pm+}$ isoscalar states coupled to a pair of gluons [24], and low-mass enhancements favored by the fragmentation process [24]. The isoscalar $C = +\Lambda\bar{\Lambda}$ threshold enhancement can be searched for in $e^+e^- \to \phi\Lambda\bar{\Lambda}$ and its spin-parity can be determined by studying the angular distribution if the data sample is large enough.

In this paper, we report the first observation of the process $e^+e^- \to \phi\Lambda\bar{\Lambda}$ analyzing data samples taken at center-of-mass (CM) energies $\sqrt{s}$ ranging from 3.51 to 4.60 GeV. The vector charmonium/charmoniumlike states are studied based on the energy-dependent cross sections, and an intermediate state in the $\Lambda\bar{\Lambda}$ system is investigated to extract information on light mesons.

II. DETECTOR AND DATA SAMPLES

The BESIII detector is a magnetic spectrometer [25] located at the Beijing Electron Positron Collider (BEPCII) [26]. The cylindrical core of the BESIII detector consists of a helium-based multilayer drift chamber (MDC), a plastic-scintillator time of flight (TOF) system, and a CsI(Tl) electromagnetic calorimeter (EMC), which are all enclosed in a superconducting solenoidal magnet providing a 1.0 T magnetic field. The solenoid is supported by an octagonal flux-return yoke with resistive plate counter muon identifier modules interleaved with steel. The acceptance of charged particles and photons is 93% over a 4π solid angle. The charged-particle momentum resolution at 1 GeV/c is 0.5%, and the dE/dx resolution is 6% for the electrons

from Bhabha scattering. The EMC measures photon energies with a resolution of 2.5% (5%) at 1 GeV in the barrel (end cap) region. The time resolution of the TOF barrel part is 68 ps, while that of the end cap part is 110 ps. The end cap TOF system was upgraded in 2015 with multigap-resistive plate chamber technology, providing a time resolution of 60 ps [27].

The experimental data used in this analysis were taken at the CM energies ranging from 3.51 GeV to 4.60 GeV as shown in Table I. Simulated samples produced with the GEANT4-based [28] Monte Carlo (MC) package which includes the geometric description of the BESIII detector and the detector response, are used to determine the detection efficiency and to estimate the background contributions. The simulation includes the beam energy spread and ISR in the e^+e^- annihilations modeled with the generator KKMC [29]. Inclusive MC simulation samples generated at $\sqrt{s} = 4.178$ GeV are used to analyze the possible background contributions. In total, these samples are 40 times larger than the data sample. They consist of

open charm production processes, ISR production of vector charmonium or charmoniumlike states, and continuum processes ($e^+e^- \rightarrow q\bar{q}$, $q = u$, d, s). The open charm production processes are generated using CONEXC, and the ISR production is incorporated in KKMC [29]. The known decay states are modeled with EvtGen [30] using branching fractions taken from the Particle Data Group (PDG) [31], and the remaining unknown decays from the charmonium states with LundCharm [32]. The final state radiations (FSR) from charged final state particles is incorporated with the PHOTOS package [33]. It should be pointed out that only $e^+e^- \rightarrow K^+K^-\Lambda\bar{\Lambda}$ is simulated in the inclusive MC samples.

The signal MC samples of $e^+e^- \rightarrow \phi\Lambda\bar{\Lambda}$ are generated with EvtGen [30] along with KKMC [29] to handle the e^+e^- annihilations and ISR production. The signal events are generated with three-body phase space (PHSP) model where the $\phi\Lambda\bar{\Lambda}$ is distributed uniformly in the phase space. The data samples used in this analysis have been collected by BESIII at 28 CM energies between 3.51 GeV and

TABLE I.   Summary of the cross section measurements of the $e^+e^- \rightarrow \phi\Lambda\bar{\Lambda}$ process at each CM energy point. Here, $\mathcal{L}_{\text{int}}$ is the integrated luminosity, N_{sig} is the number of signal events from the fit to $M(K^+K^-)$ distributions with statistical uncertainty only, ε is the efficiency, $(1 + \delta)$ is the radiative correction, and $\sigma^{\text{dress}}(\text{pb}^{-1})$ is the cross section quoted with a statistical and systematic uncertainty, respectively.

$\sqrt{s}$ (MeV)	$\mathcal{L}_{\text{int}}(\text{pb}^{-1})$	N_{sig}	ε (%)	$(1 + \delta)$	$\sigma(\text{pb})$
3510.6	366.1	4.28 ± 2.19	4.22	0.84	$0.66 \pm 0.34 \pm 0.05$
3773.0	2931.8	167.79 ± 14.29	10.93	0.89	$1.20 \pm 0.10 \pm 0.11$
3869.5	224.0	15.02 ± 3.69	12.27	0.91	$1.23 \pm 0.31 \pm 0.11$
4007.6	482.0	34.83 ± 6.28	13.90	0.95	$1.14 \pm 0.20 \pm 0.09$
4128.5	401.5	17.73 ± 4.49	13.55	1.06	$0.64 \pm 0.16 \pm 0.05$
4157.4	408.7	19.01 ± 4.95	14.22	1.02	$0.69 \pm 0.17 \pm 0.06$
4178.4	3160.0	173.23 ± 14.34	14.63	1.00	$0.76 \pm 0.07 \pm 0.07$
4188.8	565.8	29.84 ± 5.96	14.76	1.00	$0.74 \pm 0.16 \pm 0.07$
4198.9	524.6	23.57 ± 5.38	14.93	1.01	$0.62 \pm 0.13 \pm 0.05$
4209.2	573.0	26.61 ± 5.62	14.47	1.01	$0.65 \pm 0.15 \pm 0.06$
4218.7	568.9	28.75 ± 5.97	14.50	1.01	$0.64 \pm 0.14 \pm 0.06$
4226.3	1100.9	66.49 ± 8.89	15.62	1.00	$0.77 \pm 0.11 \pm 0.07$
4235.7	530.6	23.10 ± 5.23	15.01	1.03	$0.58 \pm 0.15 \pm 0.05$
4243.8	537.4	15.88 ± 4.53	14.31	1.15	$0.36 \pm 0.11 \pm 0.03$
4258.0	828.4	54.94 ± 8.17	14.56	1.11	$0.82 \pm 0.14 \pm 0.07$
4266.8	529.7	29.22 ± 6.06	14.62	1.10	$0.71 \pm 0.14 \pm 0.06$
4277.7	175.5	2.31 ± 2.07	14.15	1.09	$0.18 \pm 0.15 \pm 0.02$
4287.9	502.4	18.48 ± 4.70	14.47	1.09	$0.47 \pm 0.12 \pm 0.04$
4312.0	501.2	25.19 ± 5.75	15.54	0.97	$0.69 \pm 0.16 \pm 0.07$
4337.4	505.8	25.26 ± 5.55	16.41	0.97	$0.62 \pm 0.14 \pm 0.06$
4358.3	543.9	36.31 ± 5.80	17.09	0.96	$0.83 \pm 0.14 \pm 0.07$
4377.4	522.7	28.33 ± 5.79	17.08	0.96	$0.70 \pm 0.15 \pm 0.06$
4396.5	507.8	35.20 ± 6.32	16.89	0.97	$0.88 \pm 0.16 \pm 0.08$
4415.6	1090.7	55.73 ± 7.93	17.44	0.96	$0.59 \pm 0.09 \pm 0.05$
4436.2	569.9	35.80 ± 6.74	17.41	0.95	$0.66 \pm 0.13 \pm 0.06$
4467.1	111.1	8.31 ± 2.91	17.80	0.95	$0.91 \pm 0.30 \pm 0.08$
4527.1	112.1	7.98 ± 2.81	18.09	0.96	$0.80 \pm 0.28 \pm 0.07$
4599.5	586.9	35.10 ± 6.41	16.30	0.97	$0.73 \pm 0.14 \pm 0.06$

4.60 GeV, as listed in Table I, along with the CM energy and corresponding integrated luminosity. The total integrated luminosity is 19.5 fb^{-1}.

III. EVENT SELECTION

The selection of charged tracks is based on the following criteria. For each charged track, the polar angle in the MDC must satisfy $|\cos\theta| < 0.93$, and the point of closest approach to the e^+e^- interaction point (IP) must be within ± 20 cm in the beam direction and within 10 cm in the plane perpendicular to the beam direction. The particle identification (PID) of kaons, pions, and protons is based on the dE/dx and TOF information. Assumption of a given particle identification is based on the largest of the all PID hypotheses probabilities. The ϕ meson is reconstructed using candidate K^+K^- pairs. One $\bar{\Lambda}$ (Λ) baryon is assumed to be missing in order to improve the reconstruction efficiency. Thus we require that there should be at least one proton and one pion with opposite charge, and one K^+K^- pair in the final state.

Since the Λ baryon has a relatively long lifetime, it travels a certain distance before it decays. A vertex fit is applied to its decay products $p\pi^-$ ($\bar{p}\pi^+$) to ensure that their tracks are pointing back to the same vertex. The Λ ($\bar{\Lambda}$) baryon is reconstructed combining the $p\pi^-$ ($\bar{p}\pi^+$) final state passed the vertex fit. Then, to verify that the selected $K^+K^-\Lambda(\bar{\Lambda})$ candidates originate from the IP, another vertex fit is performed. Only events with a good quality vertex fit are retained. The flight distance between the IP and the Λ decay vertex is required to be greater than two times of its resolution. The momenta corrected by the vertex fit are used for kinematic fit.

To improve the track momentum resolution and to reduce the background, a kinematic fit is applied to the $K^+K^-\Lambda(\bar{\Lambda})$ candidates constraining the missing mass to the nominal mass of Λ. The fraction of events containing more than one Λ baryon is about 31%. For events with multiple candidates, we choose the combination with the smallest χ^2 combining the two vertex fits and the kinematic fit. The distributions of the combined χ^2 versus the invariant mass of $p\pi$ are shown in Fig. 1. To make a better comparison, the one dimensional χ^2 distribution

compared between data and MC is shown in Fig. 1 (right). The possible differences are considered as systematic uncertainty coming from the kinematic fit. The sum of the χ^2 values of the vertex and kinematic fits is required to be less than 30. The invariant mass of selected $p\pi$ final state should be within the interval $[1.112, 1.120]$ GeV/c^2, which covers about $\pm 3\sigma$ of the Λ signal region.

IV. DATA ANALYSIS

A. Signal extraction

Studies of the inclusive MC simulation indicate that the main background contribution comes from the process $e^+e^- \to (\gamma)K^+K^-\Lambda\bar{\Lambda}$, which does not peak around the ϕ signal area. It should be pointed out that at $\sqrt{s} = 4.6$ GeV, the CM energy is above the threshold of $e^+e^- \to \Lambda_c^+\bar{\Lambda}_c^-$, and there is a background contribution from $\Lambda_c^\pm \to \Lambda K^\pm$ decays. However, according to the Born cross section reported in Ref. [34], the contribution of this background in the whole fitting range (the invariant mass of K^+K^- M(K^+K^-) $\in [0.98, 1.20]$ GeV/c^2) is estimated to be only 8.8 ± 0.1 events. Other sources of background considered are found to be negligible.

To obtain the signal yields, an unbinned maximum likelihood fit is performed to the invariant mass spectrum of the K^+K^- pair for each CM energy point. The signal distribution is described by a MC-simulated shape, and the background shape is described by an inverted ARGUS [35] function whose threshold is fixed to $2m_{K^\pm}$, where $m_{K^\pm}$ is the nominal kaon mass [31]. The fit result for $\sqrt{s} = 4.178$ GeV is shown in Fig. 2 as an example, and the numbers of signal events (N_{sig}) at 28 energy points are listed in Table I.

B. Intermediate structure study

We perform a study to investigate possible intermediate structures to better estimate the reconstruction efficiency. The Dalitz plot distribution of the $\phi\Lambda\bar{\Lambda}$ candidates at $\sqrt{s} = 4.178$ GeV is shown in Fig. 3, after requiring that M(K^+K^-) $\in [1.01, 1.03]$ GeV/c^2. It is clear that most of the events in the data are deposited near the $\Lambda\bar{\Lambda}$ threshold, which is different from the PHSP MC sample generated
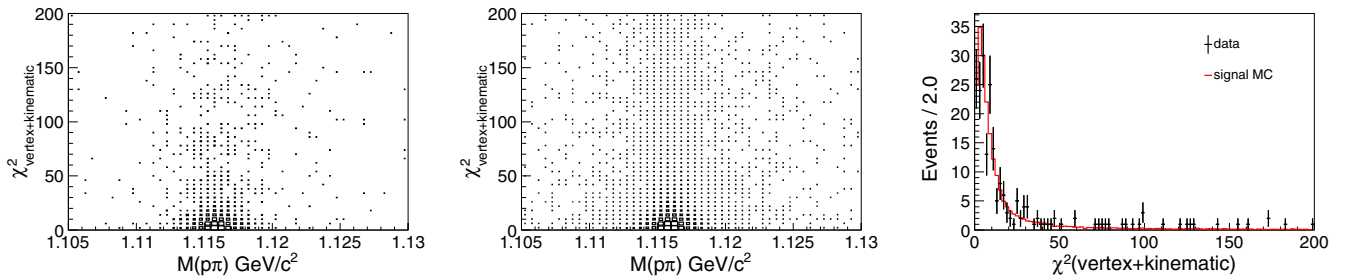

FIG. 1. Scattering plots of χ^2 versus the invariant mass of $p\pi$ from data sample summing all energy points (left) and MC simulation at 4.178 GeV (middle). Right plot is comparison of the χ^2 distribution between data and MC samples.
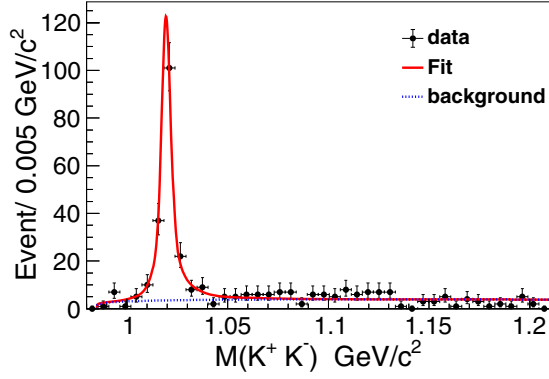
FIG. 2. Invariant mass distribution of the $\phi \to K^+K^-$ candidates for the data sample collected at $\sqrt{s} = 4.178$ GeV. The data (dots) are overlaid by the result of the fit (red solid line) described in the text. The blue dotted line represents the background component of the fit.
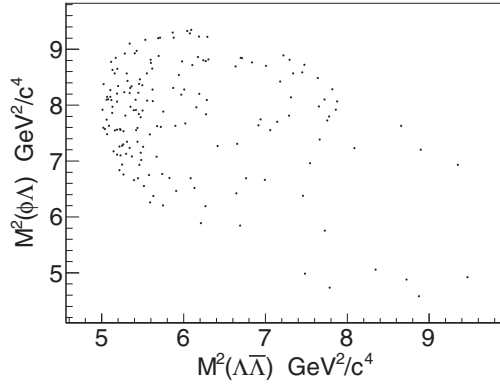

FIG. 3. Dalitz plots for the $e^+e^- \to \phi\Lambda\bar{\Lambda}$ events at $\sqrt{s} = 4.178$ GeV.

FIG. 4. Mass-dependent reconstruction efficiency (top) and resolution (bottom) curve from the signal MC study at $\sqrt{s} = 4.178$ GeV.

with a uniform distribution. Signal MC samples are generated at 28 energy points to study the reconstruction efficiency and resolutions. The efficiency and resolution curves are shown in Fig. 4 for MC samples at $\sqrt{s} = 4.178$ GeV. We can see that the reconstruction efficiency is quite smooth near the threshold and the resolution is relatively small.

The invariant mass distribution of the $\Lambda\bar{\Lambda}$ candidates for the full data sample is shown in Fig. 5. There are serval dynamics to generate such an enhancement, including final state interaction (FSI), a tail of a lower mass resonance, and so on [20,24,31]. To describe the line shape of this enhancement, an extended unbinned maximum likelihood fit is performed on all the data samples simultaneously. We first perform a fit using a Breit-Wigner function (BW) to describe the signal. Three components are considered in the fit: a near-threshold enhancement, a component distributed uniformly in PHSP, and a non-ϕ background component. The interference between the resonant signal and
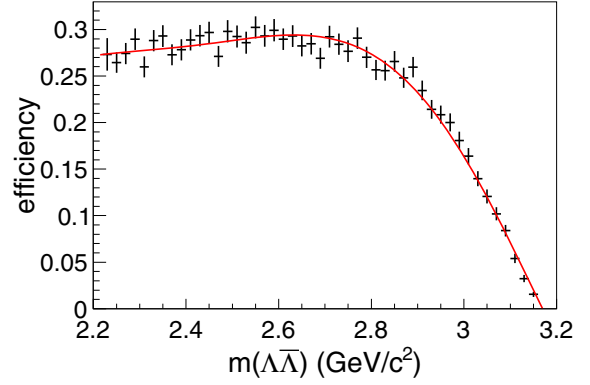
nonresonant signal is ignored here. The following formula is used to describe the line shape of the enhancement [36]

$$
\begin{aligned}
dN/dm_{\Lambda\bar{\Lambda}} \\
\propto \varepsilon(M_{\Lambda\bar{\Lambda}})(k^*)^{2l+1}f_l^2(k^*)|BW(M_{\Lambda\bar{\Lambda}})|^2(q^*)^{2L_d+1}f_{L_d}^2(q^*),
\end{aligned}
\tag{1}
$$

where $\varepsilon(M_{\Lambda\bar{\Lambda}})$ is the mass-dependent efficiency obtained from MC simulation. Here the MC sample is generated with the nonuniform angular distributions measured in data (to be described later). $M_{\Lambda\bar{\Lambda}}$ is the invariant mass of $\Lambda\bar{\Lambda}$ system,

$$
k^* \equiv \sqrt{\left(\frac{s + M_{\Lambda\bar{\Lambda}}^2 - m_\phi^2}{2\sqrt{s}}\right)^2 - M_{\Lambda\bar{\Lambda}}^2}
\tag{2}
$$

is the momentum of $\Lambda\bar{\Lambda}$ system in the e^+e^- rest frame, where m_ϕ is the nominal mass of ϕ [31],

$$
q^* \equiv \sqrt{M_{\Lambda\bar{\Lambda}}^2/4 - m^2(\Lambda)}
\tag{3}
$$

is the momentum of the Λ baryon in $\Lambda\bar{\Lambda}$ system rest frame, l is the orbital-angular momentum between ϕ and the $\Lambda\bar{\Lambda}$
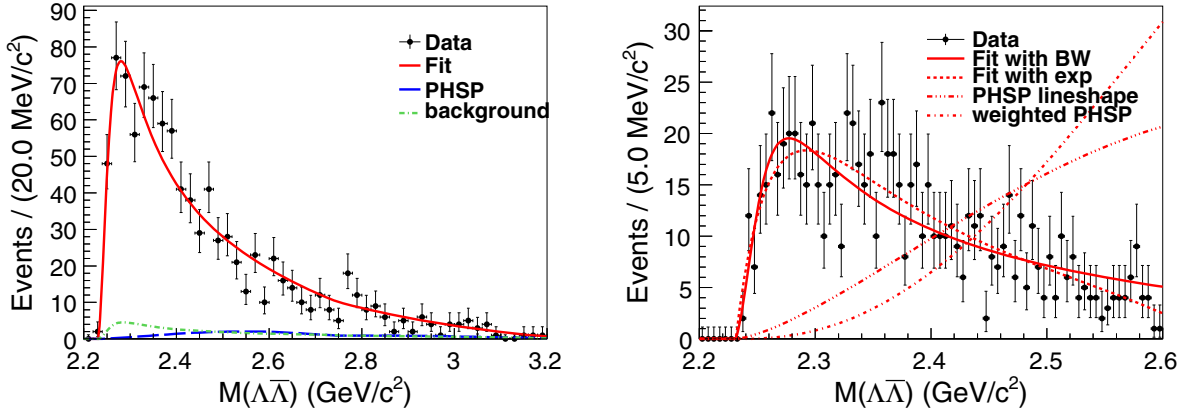
FIG. 5.   Invariant mass distribution of the $\Lambda\bar{\Lambda}$ candidates for the full data sample. The data (dots) are overlaid by the result of the fit (red solid line) described in the text. The blue long dashed line represents the PHSP components, and the green dashed-dotted line represents the background. The same distribution focusing on the lower mass range is shown in the right plot, where the red dashed line represents the fit result with the reversed exponential function, the red dash triple dotted line represents the PHSP line shape, and the red dash-dotted line represents the line shape of PHSP events weighted by the angular distribution.

system, L_d is the orbital-angular momentum between Λ and $\bar{\Lambda}$, f_L is the Blatt-Weisskopf barrier factor, with $f_0^2(z) = 1$, $f_1^2(z) = 1/(1+z)$, and $f_2^2(z) = 1/(9+3z+z^2)$. The relativistic Breit-Wigner function (with a mass-dependent width) used here is defined as

$$BW(M_{\Lambda\bar{\Lambda}}) \propto \frac{1}{M_{\Lambda\bar{\Lambda}}^2 - m^2 - im\Gamma_X}, \qquad (4)$$

where $\Gamma_X \equiv \Gamma_0 (q^*/q^0)^{2L_d+1}(m/M_{\Lambda\bar{\Lambda}})(f_{L_d}^2(q^*)/f_{L_d}^2(q^0))^2$, m and Γ_0 are the mass and width of the BW function, respectively, and q^0 is equal to q^* for $M(\Lambda\bar{\Lambda}) = m$. In the fit, the mass and width are shared parameters between all the data samples, and are left free, as well as the signal yields. The orbital-angular momentum between ϕ and the $\Lambda\bar{\Lambda}$ system is $l = 0$, and the orbital-angular momentum between the Λ and $\bar{\Lambda}$ baryons is $L_d = 1$, assuming this is a 1^{++} or 2^{++} state. Please note that even though we use a BW function here to describe the near-threshold enhancement, we are not suggesting that this enhancement is a resonant or resonantlike structure. The resolution effect is ignored here because it is relatively small compared with such a broad distribution.

The shape for PHSP signal is obtained from MC simulation. The shape of the non-ϕ background is obtained from the ϕ sideband region ($M(K^+K^-) \in [0.99, 1.005]$ or $[1.075, 1.090]$ GeV/c^2), and is parametrized with a Landau function. The number of background events is extrapolated from the sidebands to the ϕ signal region using the inverted ARGUS background function. The fit result using all data samples [37] is show in Fig. 5 (left). We also zoom in on the lower mass side to have a closer look at the rise of the enhancement, as shown in Fig. 5 (right). The mass and

width of the BW formula are fitted as (2262 ± 4) MeV/c^2 and (72 ± 5) MeV, respectively.

Alternatively, we perform a fit to estimate the rise rate near the threshold with the formula

$$dN/dm_{\Lambda\bar{\Lambda}} \propto \mathcal{P}^3(1 - e^{-\Delta M_{\Lambda\bar{\Lambda}}/p_0}), \qquad (5)$$

where $\mathcal{P}^3$ is a third-order polynomial whose parameters are free, p_0 is a free parameter, and $\Delta M_{\Lambda\bar{\Lambda}} \equiv M_{\Lambda\bar{\Lambda}} - 2m_\Lambda$. The fit result is shown in Fig. 5 (right), with $p_0 = 33 \pm 11$ MeV/c^2. Compared with the line shapes of PHSP events weighted by angular distribution and cross section from each energy point, the rising rate in data is much faster.

To further understand the nature of this enhancement, the helicity angles of the ϕ and Λ candidates are studied. The helicity angle is defined as the angle between the momentum of the ϕ or Λ in its parent's rest frame and the momentum of ϕ or Λ's parent in its grandparent's rest frame. The helicity angular distributions for events in the ϕ signal region after efficiency correction are shown in Fig. 6, combining all data samples. The unbinned maximum likelihood fit is performed simultaneously to the angular distributions, considering the same components as the ones contributing to the fit of the $M(\Lambda\bar{\Lambda})$ distribution. A fraction of each component is fixed to that obtained from the $\Lambda\bar{\Lambda}$ mass spectra fit; possible interference is not considered in the fit. The shapes of resonant signal are described with the formula constructed according to Ref. [38]. The details of the formula we used are provided in the supplementary material. The shapes of the background and PHSP signal distributions are assumed to be flat. The number of events in each component is fixed to the fit result of $M(\Lambda\bar{\Lambda})$. The fit favors the hypotheses of $J^{PC} = 1^{++}$, 2^{++}, or 2^{-+},
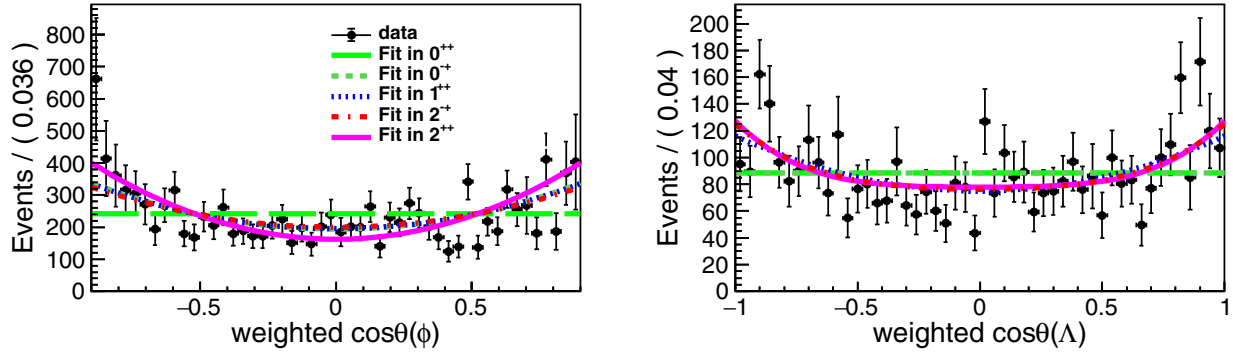
FIG. 6. Efficiency-corrected angular distribution of the ϕ (left) and Λ (right) candidates combining all the data samples and the simultaneous fit results with different hypotheses of J^{PC}. The data (dots) are overlaid by the result of the fits described in the text, the green long dashed curves are fit result for $J^{PC} = 0^{++}$, the green dashed curves are fit result for $J^{PC} = 0^{-+}$, the blue dotted curves are $J^{PC} = 1^{++}$, the red dash-dotted curves are $J^{PC} = 2^{-+}$, and the rose solid are $J^{PC} = 2^{++}$.

where the results lead to the similar fit quality. The hypothesis of this enhancement having spin-zero is rejected with significance greater than 7σ compared with other hypotheses. The fit result with different J^{PC} hypotheses are shown in Fig. 6.

Data driven reconstruction efficiencies are obtained by reweighting the signal MC samples in the generator level. The contribution of the near-$\Lambda\bar{\Lambda}$-threshold enhancement and nonuniform angular distributions measured in data are considered. The energy-dependent reconstruction efficiencies for the PHSP and the reweighted models are shown in Fig. 7. The fine structures observed in the efficiency curve are due to the deformation in the cross section line shape, which is considered in MC generation to obtain the correct ISR factor and efficiency.

C. Cross section measurement

The cross section at a certain CM energy is calculated as

$$\sigma = \frac{N_{\text{sig}}}{\mathcal{L}_{\text{int}}\mathcal{B}\varepsilon(1+\delta)}, \qquad (6)$$
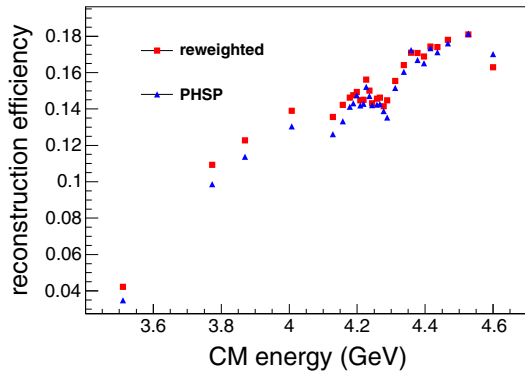

FIG. 7. Energy-dependent reconstruction efficiencies using MC samples generated using a PHSP model (blue triangle) and after reweighting the MC sample with the data distribution (red box).

where N_{sig} is the number of $\phi\Lambda\bar{\Lambda}$ signal events obtained from the fit to the $M(K^+K^-)$ distribution, $\mathcal{L}_{\text{int}}$ is the integrated luminosity, ε is a weighted value of the efficiencies from the process $e^+e^- \to \phi\Lambda\bar{\Lambda}$ where $M(\Lambda\bar{\Lambda})$ following the line shape of the near-threshold enhancement as well as the angular distributions, and the process $e^+e^- \to \phi\Lambda\bar{\Lambda}$ uniformly distributed in phase space, $\mathcal{B}$ is the product of the branching fraction of the intermediate decays $\phi \to K^+K^-$ and $\Lambda \to p\pi$, which are taken from Ref. [31], and $(1+\delta)$ is the ISR correction factor.

To obtain the proper ISR correction factor, an iterative procedure is used. First, a series of signal MC samples are generated for all energy points with a constant cross section using KKMC. The cross sections are calculated based on the reconstruction efficiencies and ISR correction factors obtained from the signal MC simulation. We use the Lowess [39] method to smooth the line shape of the measured cross sections, then we use the method introduced in Ref. [40] to get the ISR correction factors and efficiencies with the new line shape. A new series of cross sections could be obtained, and after several iterations, the cross section results become stable.

However, when the iteration is performed, the cross section results at each energy point are correlated. To take the correlation into consideration, we use pseudoexperiments. First, a large pseudodata sample is generated by sampling a Gaussian distribution, the mean value of which is the nominal cross section result, and its width is the statistical error from the fit to the data. Then, the iteration described in the previous paragraph with this new line shape is performed. The resulting cross section distributions at each energy point are fitted with Gaussian functions. Their mean and width values are taken as the final results for the cross sections and their corresponding uncertainties, respectively. The final results are shown in Fig. 8, and listed in Table I, including the statistical and systematic uncertainties.
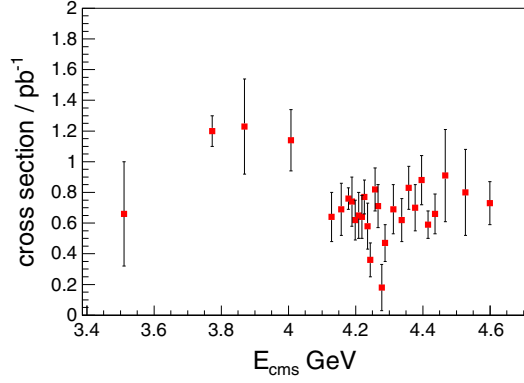
FIG. 8. Energy-dependent cross section distribution, where dots with error bars correspond to the cross section measurements at each CM energy point.

V. SYSTEMATIC UNCERTAINTIES

A. Uncertainties on cross sections

The systematic uncertainties include contributions from luminosity, tracking, PID efficiencies of the kaons, Λ reconstruction, radiative correction factor associated with the efficiency, background, and branching fractions of the intermediate states.

The integrated luminosity is measured using Bhabha scattering events, with an uncertainty smaller than 1.0% [41]. The uncertainty related to the tracking efficiency of kaons is estimated to be 1.0%, and the uncertainty arising from the kaon PID efficiency is determined to be 1.0% using a control sample $e^+e^- \to K^+K^-\pi^+\pi^-$. With the control sample, the tracking or PID requirement efficiency is separately measured in the MC simulation sample and in the data sample. The difference between the efficiencies from MC simulation and data samples is taken as the systematic uncertainty.

The systematic uncertainty due to the Λ reconstruction efficiency including the tracking and PID of its decay products $p\pi$, as well as the decay length requirement, is studied with the control sample $\Lambda_c \to \Lambda + X$ decays. The resulting systematic uncertainty is 1.1% [42].

The systematic uncertainty due to the $\Lambda(\bar{\Lambda})$ and ϕ mass window selection criteria accounts for the mass resolution discrepancy between the MC simulation and experimental data. The ϕ and Λ mass distributions from signal MC sample and data are fitted with double-Gaussian functions and compared with each other. The difference between the fit results is negligible.

For the uncertainty due to the ISR correction factor, we change the line shape with a power law function $1/s^n$. The difference between the nominal result and the alternative parametrization is taken as the systematic uncertainty. To estimate the systematic uncertainty related to the background model, we vary the fit range of the $M(K^+K^-)$ distribution. We also use a second-order polynomial as an alternative background model. The largest value among all

variations is taken as systematic uncertainty for this source. Due to limited sample sizes at most CM energy points, the uncertainty from the data sample collected at $\sqrt{s} = 4.178$ GeV is used for all the data sets.

The uncertainty of the kinematic fit is estimated by comparing the reconstruction efficiency before and after the helix parameter correction using the method described in Ref. [43]. It should be pointed out that the reconstruction efficiency after the helix parameter correction is used as the nominal result. The uncertainties of the branching fractions are taken from the PDG [31].

The summary of the systematic uncertainties at $\sqrt{s} = 4.178$ GeV is presented in Table II.

B. Uncertainties on $M(\Lambda\bar{\Lambda})$ line shape

The systematic uncertainties for the mass and width of the BW formed line shape include those from the mass calibration, efficiency curve, signal parametrization, and background estimation.

To calibrate the mass component, a maximum likelihood fit of the K^+K^- invariant mass distributions is performed for all the data samples. The difference between the fitted mass and the known mass of the ϕ meson [31] is 0.4 MeV/c^2. According to the conservation of energy and momentum, the difference on the $\Lambda\bar{\Lambda}$ side should be 0.3 MeV/c^2. This value is taken as the systematic uncertainty.

To evaluate the systematic uncertainty from the efficiency curve estimation, we use an unweighted PHSP MC sample instead of the nominal one to extract the efficiency curve. The changes on the mass and width (0.6 MeV/c^2 and 8.0 MeV, respectively) are taken as the systematic uncertainties.

To account for the systematic uncertainty from the signal model, we change the parametrization form from a Landau to a BW function. The differences between the two parametrizations, 22.9 MeV/c^2 and 13.5 MeV, are taken as the systematic uncertainties on the mass and width, respectively. Another source of uncertainty in the signal

TABLE II. Summary of the systematic uncertainties for the cross section measurements using $\sqrt{s} = 4.178$ GeV data as an example.

Source	(%)
Luminosity	1.0
Tracking	2.0
PID	2.0
Λ reconstruction	1.1
ISR factor	5.6
Kinematic fit	1.0
Branching fraction	0.8
Background model	2.6
Total	7.1

TABLE III. Summary of systematic uncertainties for the $M(\Lambda\bar{\Lambda})$ near-threshold enhancement lineshape parameters.

Source	Mass (MeV/c^2)	Width (MeV)	p_0 (MeV/c^2)
Mass calibration	0.3	⋯	⋯
Efficiency curve	0.6	8.0	⋯
Signal model	22.9	13.5	⋯
Quantum number	1.7	36.0	⋯
Background estimation	3.1	1.2	0.4
Background model	15.9	18.0	⋯
Fit range	⋯	⋯	5.5
Total	28.1	43.2	5.5

parametrization is the quantum number assumption. We change the assignment of $l/L_d = 0/1$ to $1/2$. The differences on the mass and width, 1.7 MeV/c^2 and 36.0 MeV, are taken as the systematic uncertainties. For the background estimation, we get different yields by varying the fit range of the K^+K^- invariant mass distributions and repeating the fit. The differences on the mass and width, 3.1 MeV/c^2 and 1.2 MeV, respectively, are taken as the systematic uncertainties. Replacing the background parametrization with a BW function leads to changes in the measurement of the mass and width, 15.9 MeV/c^2 and 18.0 MeV, which are taken as the systematic uncertainties from the background model.

Table III summarizes these three sources of uncertainties. The sum of all the above uncertainties in quadrature, 28.1 MeV/c^2 and 43.2 MeV for the mass and width, respectively, are taken as the total uncertainties.

The systematic uncertainty for the reversed exponential parameter comes from similar sources. We broaden or narrow the fit range by 0.02 GeV, and the change of the exponential parameter 4.8 is taken as systematic uncertainty. The efficiency curve is flat near the threshold, which will not affect the exponential parameter. The mass calibration will not change the line shape so this source is also ignored. We vary the background estimation and the background shape—the largest changes of the exponential parameter is 0.4. The uncertainties are also summarized in Table III. The sum of all the above uncertainties in quadrature, 4.8, is taken as the total systematic uncertainty.

VI. SUMMARY AND DISCUSSION

In summary, we observe the $e^+e^- \to \phi\Lambda\bar{\Lambda}$ process for the first time with data samples at CM energies ranging from 3.51 GeV to 4.60 GeV. The energy-dependent cross sections of $e^+e^- \to \phi\Lambda\bar{\Lambda}$ are measured. Due to the limited sample sizes, we cannot resolve the composition of the resonance structure, and the line shape might not be simply described with a continuum process parametrized as $1/s^n (n = 3.3 \pm 0.3)$.

Moreover, a near-threshold enhancement is observed on $\Lambda\bar{\Lambda}$ with a significance greater than 25σ compared with the pure phase space distribution. By fitting the line shape with a BW function, we obtain the mass and width as $(2262 \pm 4 \pm 28)$ MeV/c^2 and $(72 \pm 5 \pm 43)$ MeV, repectively, where the first uncertainties are statistical and the second ones are systematic. By fitting the line shape with a reversed exponential function, we obtain the rising rate (exponential parameter) as $33 \pm 11 \pm 6$ MeV/c^2.

According to the helicity-angle study, the quantum numbers of the $\Lambda\bar{\Lambda}$ system $J^{PC} = 0^{++/-+}$ is rejected with a significance of 7σ. The interpretation of the $\Lambda\bar{\Lambda}$ system originating from a decay $\eta(2225) \to \Lambda\bar{\Lambda}$ is rejected. The J^{PC} quantum numbers could be 2^{++}, 2^{-+}, or 1^{++}, but they cannot be distinguished because of the limited data sample sizes. Another interpretation of a lower mass resonance is that this could be a $f_2(2300)$ meson. However, according to previous measurements using the decay modes $J/\psi \to \gamma\phi\phi$ and $J/\psi \to \gamma\Lambda\bar{\Lambda}$ [44,45], the $f_2(2300)$ meson is more likely to decay into a $\phi\phi$ final state rather than to $\Lambda\bar{\Lambda}$. The cross sections of the $e^+e^- \to \phi\phi\phi$ process are measured [46] at BESIII with similar cross sections to those of the $e^+e^- \to \phi\Lambda\bar{\Lambda}$ process, but no structure around 2.23 GeV/c^2 is observed in the $\phi\phi$ mass spectrum. Therefore the interpretation of $f_2(2300) \to \Lambda\bar{\Lambda}$ is also rejected.

This enhancement does not match any known resonance [31] seen before, and could be the same thing observed in $B \to K\Lambda\bar{\Lambda}$ decays [22]. If so, the theoretical explanation, an isoscalar state with $J^{PC} = 0^{\pm+}$ coupled to a pair of gluons [24], could be discarded since the hypothesis implying quantum numbers 0^{-+} is rejected based on the angular-distribution study. Also, the author of Ref. [24] implies that the observed threshold enhancements in low-mass baryon-antibaryon systems might not be limited to the ordinary quantum numbers of the $q\bar{q}$ system. Further studies of the $\Lambda\bar{\Lambda}$ system would be helpful to understand the nature of this threshold enhancement. For example, a search for a threshold enhancement in the $e^+e^- \to \eta\Lambda\bar{\Lambda}$ process could provide a crucial test because the states produced in this mode have the exact opposite C parity to the state in our analysis.

[1] For recent reviews, see N. Brambilla, S. Eidelman, C. Hanhart, A. Nefediev, C. P. Shen, C. E. Thomas, A. Vairo, and C. Z. Yuan, Phys. Rep. **873**, 1 (2020); F. K. Guo, C. Hanhart, U. G. Meißner, Q. Wang, Q. Zhao, and B. S. Zou, Rev. Mod. Phys. **90**, 015004 (2018); H. X. Chen, W. Chen, X. Liu, and S. L. Zhu, Phys. Rep. **639**, 1 (2016); N. Brambilla *et al.*, Eur. Phys. J. C **71**, 1534 (2011).

[2] B. Aubert *et al.* (*BABAR* Collaboration), Phys. Rev. Lett. **95**, 142001 (2005).

[3] X. L. Wang *et al.* (Belle Collaboration), Phys. Rev. Lett. **99**, 142002 (2007).

[4] B. Aubert *et al.* (*BABAR* Collaboration), Phys. Rev. Lett. **98**, 212001 (2007).

[5] Q. He *et al.* (CLEO Collaboration), Phys. Rev. D **74**, 091104 (2006).

[6] C. Z. Yuan *et al.* (Belle Collaboration), Phys. Rev. Lett. **99**, 182004 (2007).

[7] M. Ablikim *et al.* (BESIII Collaboration), Phys. Rev. Lett. **118**, 092001 (2017).

[8] M. Ablikim *et al.* (BESIII Collaboration), Phys. Rev. Lett. **118**, 092002 (2017).

[9] C. Z. Yuan, Chin. Phys. C **38**, 043001 (2014).

[10] M. Ablikim *et al.* (BESIII Collaboration), Phys. Rev. D **99**, 091103 (2019).

[11] M. Ablikim *et al.* (BESIII Collaboration), Phys. Rev. Lett. **122**, 102002 (2019).

[12] M. Ablikim *et al.* (BESIII Collaboration), Phys. Lett. B **771**, 45 (2017).

[13] M. Ablikim *et al.* (BESIII Collaboration), Phys. Rev. D **99**, 072005 (2019).

[14] M. Ablikim *et al.* (BESIII Collaboration), Phys. Rev. Lett. **124**, 032002 (2020).

[15] L. Maiani, V. Riquer, F. Piccinini, and A. D. Polosa, Phys. Rev. D **72**, 031502 (2005).

[16] M. Ablikim *et al.* (BESIII Collaboration), Phys. Rev. Lett. **119**, 072001 (2017).

[17] M. Ablikim *et al.* (BESIII Collaboration), Chin. Phys. C **44**, 040001 (2020).

[18] L. Zhao, N. Li, S. L. Zhu, and B. S. Zou, Phys. Rev. D **87**, 054034 (2013).

[19] M. Ablikim *et al.* (BESIII Collaboration), Phys. Rev. D **97**, 032013 (2018).

[20] J. Z. Bai *et al.* (BES Collaboration), Phys. Rev. Lett. **91**, 022001 (2003).

[21] J. T. Wei *et al.* (Belle Collaboration), Phys. Lett. B **659**, 80 (2008).

[22] Y. W. Chang *et al.* (Belle Collaboration), Phys. Rev. D **79**, 052006 (2009).

[23] Y. Nambu and G. Jona-Lasinio, Phys. Rev. **122**, 345 (1961).

[24] J. L. Rosner, Phys. Rev. D **68**, 014004 (2003).

[25] M. Ablikim *et al.* (BESIII Collaboration), Nucl. Instrum. Methods Phys. Res., Sect. A **614**, 345 (2010).

[26] C. H. Yu *et al.*, *Proceedings of IPAC2016*, Busan, Korea, 2016, https://doi.org/10.18429/JACoW-IPAC2016-TUYA01.

[27] X. Li *et al.*, Radiat. Detect. Technol. Methods **1**, 13 (2017); Y. X. Guo *et al.*, Radiat. Detect. Technol. Methods **1**, 15 (2017).

[28] S. Agostinelli *et al.* (GEANT4 Collaboration), Nucl. Instrum. Methods Phys. Res., Sect. A **506**, 250 (2003).

[29] S. Jadach, B. F. L. Ward, and Z. Was, Comput. Phys. Commun. **130**, 260 (2000); Phys. Rev. D **63**, 113009 (2001).

[30] D. J. Lange, Nucl. Instrum. Methods Phys. Res., Sect. A **462**, 152 (2001); R. G. Ping, Chin. Phys. C **32**, 243 (2008).

[31] P. A. Zyla *et al.* (Particle Data Group), Prog. Theor. Exp. Phys. (**2020**), 083C01.

[32] J. C. Chen, G. S. Huang, X. R. Qi, D. H. Zhang, and Y. S. Zhu, Phys. Rev. D **62**, 034003 (2000); R. L. Yang, R. G. Ping, and H. Chen, Chin. Phys. Lett. **31**, 061301 (2014).

[33] P. Golonka and Z. Was, Eur. Phys. J. C **45**, 97 (2006).

[34] M. Ablikim *et al.* (BESIII Collaboration), Phys. Rev. Lett. **120**, 132001 (2018).

[35] H. Albrecht *et al.* (ARGUS Collaboration), Phys. Lett. B **241**, 278 (1990).

[36] M. Ablikim *et al.* (BESIII Collaboration), Phys. Rev. Lett. **112**, 022001 (2014).

[37] See Supplemental Material at http://link.aps.org/supplemental/10.1103/PhysRevD.104.052006 for energy dependent fit results to $M(\Lambda\bar{\Lambda})$ and formalism of helicity angular distribution.

[38] S. U. Chung, Phys. Rev. D **57**, 431 (1998).

[39] W. S. Cleveland, J. Acoust. Soc. Am. **74**, 829 (1979).

[40] W. Sun, T. Liu, M. Jing, L. Wang, B. Zhong, and W. Song, Front. Phys. (Beijing) **16**, 64501 (2021).

[41] M. Ablikim *et al.* (BESIII Collaboration), Chin. Phys. C **39**, 093001 (2015).

[42] M. Ablikim *et al.* (BESIII Collaboration), Phys. Rev. Lett. **121**, 062003 (2018).

[43] M. Ablikim *et al.* (BESIII Collaboration), Phys. Rev. D **87**, 012002 (2013).

[44] M. Ablikim *et al.* (BESIII Collaboration), Phys. Rev. D **93**, 112011 (2016).

[45] M. Ablikim *et al.* (BESIII Collaboration), Phys. Rev. D **86**, 032008 (2012).

[46] M. Ablikim *et al.* (BESIII Collaboration), Phys. Lett. B **774**, 78 (2017).